JOURNAL OF MATERIALS SCIENCE 25 (1990) 1675–1681

The effect of thermal treatment on the structure and fine structure of Cu–Zn–Al martensite

JIANIAN GUI, CHANGHONG LUO, HEGE ZHANG, WEI HU, RENHUI WANG
Department of Physics, Wuhan University, Wuhan 430072, People's Republic of China

The effect of thermal treatment on the structure and fine structure of CU–17.4Zn–13.0Al (at%) martensite has been studied using X-ray powder diffraction and transmission electron microscopy. It has been found that when the directly-quenched $M18R_1$ martensite is aged at increasing temperatures, the structure parameters and x-parameter tend evidently towards the values of the $N18R_1$ martensite, while the DO_3-derived long-range order parameter S is not changed substantially. The activation energy of the structure parameter variation process of the $18R_1$ martensite during aging has been measured to be 58 kJ mol^{-1} (0.60 eV) for the directly-quenched specimen using the X-ray reflection splitting data. The aging kinetics of the step-quenched martensite is much lower compared with the directly-quenched martensite. Moreover, the anti-phase domain size of the step-quenched martensite inherited from the parent phase is much larger than that of the directly-quenched and the aged martensites. Based on our observations the mechanisms of the aging and stabilization of martensite are discussed.

1. Introduction

Recently, the aging and stabilization of Cu–Zn–Al martensite have been widely studied (see the review by Ahlers [1]). The structure, fine structure and hence the behaviour of the aging and stabilization of martensite are dependent on the thermal pretreatment. In order to explore the mechanisms of the martensite stabilization it is warranted to study the variation of the structure and fine structure of Cu–Zn–Al martensite during aging and the effect of thermal treatment on the structure and fine structure of the martensite.

X-ray diffraction studies have shown that the monoclinic 9R or $18R_1$ type martensite changes its lattice parameters during aging in the martensite state: the monoclinic angle β tends to 90° while a increases and b decreases [2–6]. At the same time the x-parameter changes towards the value $\frac{1}{3}$ characteristic of the so-called normal $18R_1$ ($N18R_1$) [4]. All these mean a decrease of the monoclinicity. A common explanation for this is that such changes indicate a change in the DO_3-derived order inherited from the DO_3 order in the parent phase [7]. But there are two opposite suppositions: that the decrease of the monoclinicity corresponds firstly to the increase of the DO_3-derived order [3, 8, 9], and secondly to the decrease of the order degree of the martensite [10–12]. In spite of this discrepancy there has been so far only one work [13] measuring directly the variation of the B2-derived ordering degree of martensite during aging.

There have been extensive transmission electron microscopy (TEM) studies of the fine structure of Cu–Zn–Al martensite including the size of the B2- and DO_3-derived domains [10], vacancy clusters [14], dislocation loops [8], precipitation [8, 14, 15] stacking fault structure [8, 10, 16] and the x-parameter [4]. Furthermore, the domain structure in the parent phase of a Cu–Zn–Al alloy [17] and Cu–Al–Ni alloys [18] were also observed using TEM. All these TEM observations and the measurement of the activation energy of the stabilization process of Cu–Zn–Al martensite using different methods [1, 10, 19] have helped to acquire deeper understanding of the mechanisms of Cu–Zn–Al martensite stabilization.

In the present study the effect of thermal treatment on the structure and fine structure of Cu–17.4Zn–13.0Al (at%) martensite, especially the variation of the lattice parameters, the x-parameter and the long-range DO_3-derived order parameter S during martensite aging have been studied by using X-ray powder diffraction and TEM. Moreover, the activation energy of the variation of the lattice parameters during aging in the martensite state has been measured. Based on these observations the mechanisms of the aging and stabilization of Cu–Zn–Al martensite are discussed.

2. Specimen preparation and experimental methods

For convenience of studying the aging process in the martensite state, Cu–17.4Zn–13.0Al (at%) alloy with higher transition temperature was prepared using raw materials of industrial purity. The transition temperatures of this alloy when step-quenched at 433 K are M_s = 388 K, M_f = 325 K, A_s = 349 K and A_f = 404 K.

0022–2461/90 $03.00 + .12

TABLE I Thermal treatments of specimens

Specimen	Thermal treatment
A Step-quenched	Solid-solution treated at 1073 K for 5 min, quenched into an oil bath at 433 K for 4 min, and then quenched into cold water.
B Directly-quenched	Solid-solution treated at 1073 K for 5 min, then quenched into ice-water directly.
C Aged at 463 K	Directly-quenched as above, heated with the furnace together from room temperature to 463 K and held 10 min
D Aged at 533 K	As above, but to 533 K and held 5 min.

Plate specimens and filings enveloped in a copper or beryllium bronze foil were subjected to different thermal treatments listed in Table I. Table I shows also the designation of each type of specimen suffering different thermal treatments. TEM foils were prepared from plate specimen first by chemical thinning at room temperature (RT) in a solution of $HCl:HNO_3:H_3PO_4 = 1:4:5$ and then by twin jet electropolishing in a D2 solution at RT. Heat-treated filings were rinsed in acetone using an ultrasonic cleaner as specimens for X-ray powder diffraction studies.

TEM observation was performed using a JEOL JEM-100CX (II) transmission electron microscope equipped with a double tilting goniometer, operated at 120 kV. A tilting experiment was conducted for obtaining a series of electron diffraction patterns (EDPs) in order to identify the structure type of the martensite [20]. (2 2 8) and (1 1 1) diffraction spots of the $18R_1$ martensite were selected for the dark field imaging displaying the antiphase domains of the B2- and DO_3-derived ordering, respectively.

Room temperature and high temperature X-ray powder diffraction patterns were obtained by using copper target and graphite monochromator. For the quantitative measurement of the integrated intensities of the DO_3-derived superreflection (0 1 9), and of the fundamental reflections (1, 2, 10) and ($\bar{2}$, 0, 10), the step-scan method was used. The degree of splitting of line-pairs such as (1, 2, 10)–($\bar{2}$, 0, 10) was expressed [3] by the so-called splitting parameter

$$\varrho = \sin^2\theta(\bar{2}, 0, 10) - \sin^2\theta(1, 2, 10) \quad (1)$$

with $\theta(\bar{2}, 0, 10)$ and $\theta(1, 2, 10)$ being the Bragg angles. The method of obtaining the lattice parameters a, b, c and β of the monoclinic $18R_1$ martensite and its x-parameter was described in a previous paper [4]. From these parameters one can calculate the angle φ between lines connecting the nearest neighbours in the basal plane of the $18R_1$ martensite as follows:

$$\varphi = 2\tan^{-1}(b/(2a)) \quad (2)$$

The value $\varphi = 60°$ corresponds to the hexagonal close packed distribution of atoms in the basal plane.

The relative intensity of (hkl) reflection in an X-ray powder diffraction pattern is expressed as (see Appendix)

$$I = \begin{cases} nS^2|F_{hkl}|^2(1 + \cos^2 2\theta)/(\sin^2\theta\cos\theta) \\ \quad \text{for } DO_3\text{-derived superlattice reflections} \\ n|F_{hkl}|^2(1 + \cos^2 2\theta)/(\sin^2\theta\cos\theta) \\ \quad \text{for fundamental reflections} \end{cases} \quad (3)$$

with n being the multiplicity, S the degree of long range DO_3-derived order, when the B2-derived order is complete, F_{hkl} the structure factor for the perfectly ordered $18R_1$ martensite and θ the bragg angle of (hkl) reflection. From Equation 3 the degree of the DO_3-derived order may be calculated by measuring the relative intensities of the superlattic reflection (0 1 9) and the fundamental reflections (1, 2, 10)–($\bar{2}$, 0, 10) as follows:

$$I_1/(I_2 + I_3) = cS^2 \quad (4)$$

with

$$c = \frac{n_1|F_1|^2 \dfrac{1 + \cos^2 2\theta_1}{\sin^2\theta_1\cos\theta_1}}{n_2|F_2|^2 \dfrac{1 + \cos^2 2\theta_2}{\sin^2\theta_2\cos\theta_2} + n_3|F_3|^2 \dfrac{1 + \cos^2 2\theta_3}{\sin^2\theta_3\cos\theta_3}} \quad (5)$$

where subscripts 1, 2 and 3 correspond respectively to the indices (0 1 9), (1, 2, 10) and ($\bar{2}$, 0, 10).

3. Experimental results

3.1. Identification of the structure type of martensite

Fig. 1 shows a part of the X-ray powder diffraction pattern of the directly-quenched specimen. The inset shows the (1 1 1) and (0 1 9) reflections measured by means of step-scan, whose appearance indicates the martensite being the $18R_1$ type arising from the DO_3 order parent phase. Moreover, some weak reflections belonging to the parent phase β_1 and the α-phase are also discernible. Fig. 2 displays electron diffraction patterns obtained by tilting the specimen around the **c*** axis of the $M18R_1$ martensite in a directly-

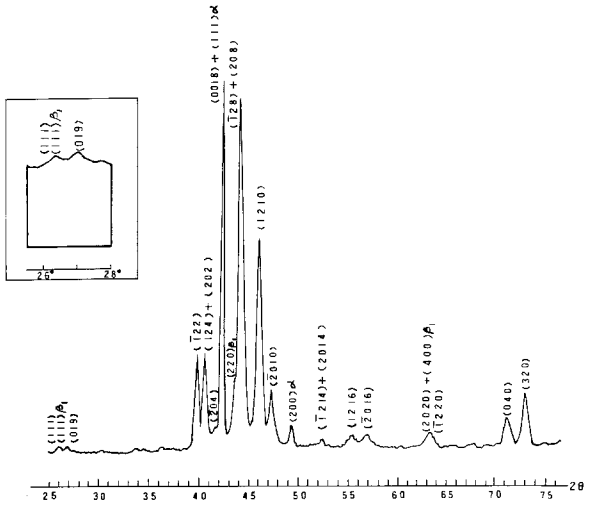

Figure 1 Part of the X-ray powder diffraction pattern of the directly-quenched specimen.

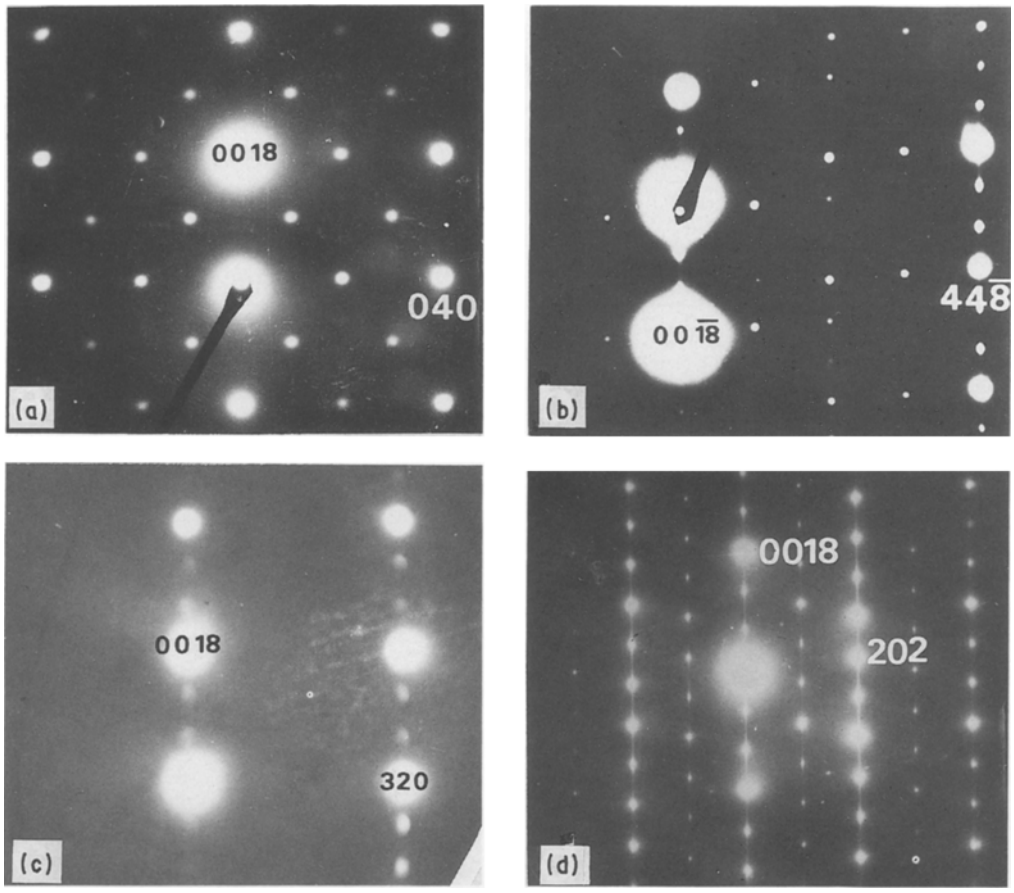

Figure 2 EDPs obtained by tilting about the **c*** axis of the $M18R_1$ martensite directly-quenched and held at room temperature for less than 3 h. (a) [1 0 0] zone; (b) [1 $\bar{1}$ 0] zone; (c) [2 $\bar{3}$ 0] zone; (d) [0 $\bar{1}$ 0] zone.

quenched alloy which was then held at RT for less than 3 h before TEM observation. The non-vanishing of the (1, 0, 10 + 6*m*)(*m* is an integer) reflections in the [0 $\bar{1}$ 0] zone, of the (2, 2, 8 + 6*m*) reflections in the [1 $\bar{1}$ 0] zone, and of the (0, 2, 18*m*) reflections in the [1 0 0] zone indicates the B2-derived order of the martensite. On the other hand, the appearance of the (1, 1, 1 + 6*m*) and (3, 3, 9 + 6*m*) reflections in the [1 $\bar{1}$ 0] zone and of the (0, 1, 9 + 18*m*) and (0, 3, 9 + 18*m*) reflections in the [1 0 0] zone indicates that the martensite is $18R_1$ type of the DO_3-derived order [20]. Furthermore, the appearance of (3 2 6) and (3, 2, 12) reflections in the [2 $\bar{3}$ 0] zone indicates the modified type of the martensite ($M18R_1$). Our observations show that the martensite, not only in the step-quenched and the aged specimens, but also in the directly-quenched specimen is of the $18R_1$ type. This means the rapid quenching can not completely suppress the B2 → DO_3 transition in the parent phase.

3.2. Structure parameters and fine structures of martensites in differently treated specimens

From the X-ray powder diffraction patterns of specimens treated as listed in Table I, the splittings $\Delta(2\theta)$ of the line-pairs (1, 2, 10)–($\bar{2}$, 0, 10) and (3 2 0)–(0 4 0), the lattice parameters *a*, *b*, *c*, β and φ, and the values of the *x*-parameter have been obtained and are listed in Table II. Table II shows that for the step-quenched martensite, line-pairs have the largest splitting, and the angles β and φ and the *x*-parameter deviate from 90°, 60° and $\frac{1}{3}$ respectively most severely. The directly-quenched martensite possesses less deviations compared with the step-quenched one. With the increase of the aging temperature, the splittings tend to 0, $\beta \rightarrow 90°$, $\varphi \rightarrow 60°$, and $x \rightarrow \frac{1}{3}$, that is, $M18R_1$ martensite tends to $N18R_1$ martensite. Moreover, the [2 $\bar{3}$ 0] zone EDPs of these specimens show that the relative intensities of (3 2 6) and (3, 2, 12) decrease tending to zero with the increase of the

TABLE II Structure parameters of $18R_1$ martensite after different thermal treatments

Specimen	$\Delta(2\theta)$ (deg)		Lattice parameters					*x*-parameter
	$\bar{2}$ 0 1 0 1 2 1 0	0 4 0 3 2 0	*a* (nm)	*b* (nm)	*c* (nm)	β (deg)	φ (deg)	
A	1.47	2.14	0.4450	0.5315	3.8345	89.05	61.69	0.349
B	1.16	1.67	0.4470	0.5300	3.8380	89.24	61.32	0.346
C	0.56	0.98	0.4485	0.5260	3.8395	89.58	60.78	0.340
D	0.29	0.35	0.4500	0.5225	3.8330	89.76	60.28	0.337

TABLE III Characteristics of the fine structure of the $18R_1$ martensite after different thermal treatments

Specimen	Substructure	Relative intensities of (3 2 6) and (3, 2, 12) reflections	B2 domain size (nm)	DO_3 domain size (nm)
Step-quenched	Larger basal plane twin density	Medium	430	56
Directly-quenched	Larger stacking fault density	Weak	130	18
Directly-quenched and then aged at T		Weaker, decreases with the increase of T	130	18

ageing temperature. This fact is consistent with above observations.

TEM observations and the selected area electron diffraction have shown that there are many irregular stacking faults on the basal plane and twins with the basal plane as their mirror plane for all specimens differently treated as listed in Table I. Nonetheless, the statistics of the TEM observations show that the directly-quenched specimen possesses larger stacking fault density as compared with other specimens, and the step-quenched specimen possesses larger basal plane twin density as compared with other specimens.

TEM dark field photographs as shown in Fig. 3 reveal that the size of the B2-derived order domains is much larger than the DO_3-derived, and both the B2- and the DO_3-derived domain size of the step-quenched martensite is larger than the directly-quenched and the directly-quenched and aged martensites. All these characteristics of the fine structure of $18R_1$ martensite as revealed by using TEM are summarized in Table III.

In order to compare the aging process of the directly-quenched martensite with that of the step-quenched martensite, the X-ray diffraction patterns of the as-step-quenched specimen, the specimen step-quenched and then aged at RT for 1 year, and the specimen step-quenched and then aged at 345 K (lower than A_s = 349 K) for 49 h, were compared. In contrast with the directly-quenched martensite, the X-ray diffraction pattern of the step-quenched martensite does not change during aging described as above.

3.3. Aging kinetics investigation using high temperature X-ray diffraction

The variation of the X-ray diffraction pattern, especially of the splitting parameter ϱ, of the directly-quenched powder specimens during the aging process at 444, 453, 465, 473 and 493 K were investigated *in situ* by using high temperature attachment. The intensities of reflections of the β_1 parent phase and the α-phase are not changed during aging, which indicates the aging is in the martensite state. On the other hand, the splitting parameter decreases during aging, and the higher the aging temperature, the faster is the decrease of the splitting parameter (see Fig. 4). When

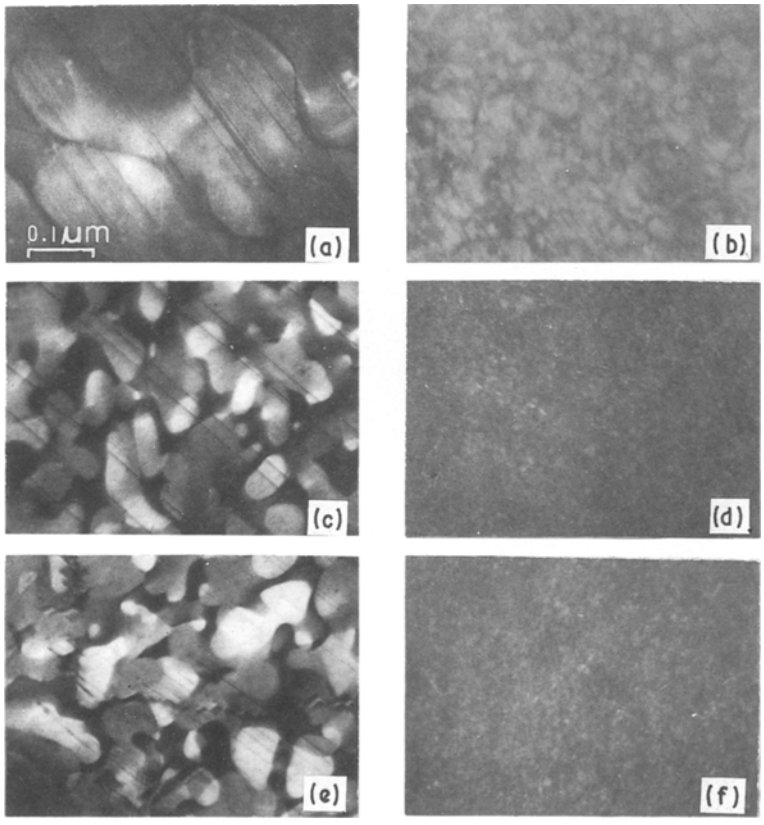

Figure 3 Domains of the $18R_1$ martensite after different thermal treatments: (a), (c) and (e): (2 2 8) dark field imaging showing B2-derived domains; (b), (d) and (f): (1 1 1) dark field imaging showing DO_3 derived domains. (a) and (b): step-quenched; (c) and (d): directly-quenched; (e) and (f): directly-quenched and aged at 493 K.

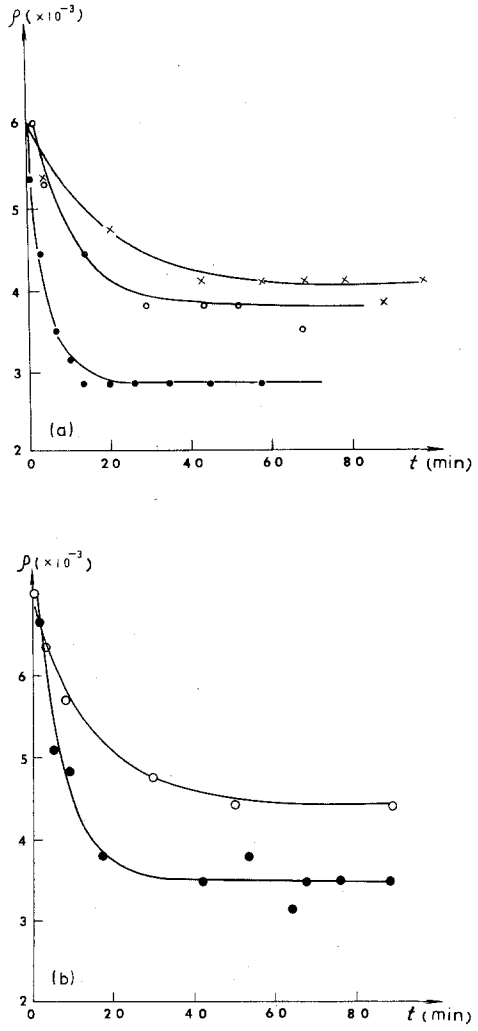

Figure 4 Variation of the splitting parameter ρ as a function of the aging time t for several aging temperatures T. (a) ×, 444 K; ○, 465 K; ●, 493 K. (b) ○, 453 K, ●, 473 K.

cooling the aged martensite, the coalesced line-pairs do not split again. These $\varrho(t)$ values can be fitted according to the following empirical equation:

$$\varrho(t) = \varrho_\infty + (\varrho_0 - \varrho_\infty) \exp(-t/\tau(T)) \quad (6)$$

with ϱ_0, $\varrho(t)$ and ϱ_∞ being the values of the splitting parameter respectively at the beginning, at time t and at the end of the aging process. The fitted values of the relaxation time $\tau(T)$, as listed in Table IV, are longer for lower aging temperature T which means that the martensite aging is a thermally activated process. Supposing

$$\tau = \tau_0 \exp(Q/(RT)) \quad (7)$$

and by plotting ln τ against $1/T$ (see Fig. 5) the value of the activation energy $Q = 58\,\mathrm{kJ\,mol^{-1}}$ (0.60 eV) of the martensite aging process has been obtained.

3.4. Effect of thermal treatment on the degree of DO_3-derived order of martensite

For the four types of thermal treatments as listed in Table I, coefficients c have been calculated by substituting related values into the right-hand side of Equation 5. After quantitatively measuring the integrated intensities I_1, I_2 and I_3 for reflections (0 1 9), (1, 2, 10) and ($\bar{2}$, 0, 10) respectively, the values of the degree of DO_3-derived order S of the $18R_1$ martensite have been determined by using Equation 4 and are listed in Table V. Table V shows that step-quenched martensite possesses a higher degree of DO_3-derived long-range order than directly-quenched martensite and the degree of DO_3-derived order of the directly-quenched martensite does not change substantially after aging.

TABLE IV Relaxation time τ at different aging temperatures

T (K)	444	453	465	473	493
τ (min)	19.34	14.56	9.86	7.15	4.70

TABLE V Intensity ratios $I_1/(I_2 + I_3)$ and the DO_3-derived order degrees S of the $18R_1$ martensite after different thermal treatments

Specimen	$I_1/(I_2 + I_3)$	$c = (I_1/(I_2 + I_3))/S^2$	S
A	0.0240	0.0379	0.80 ± 0.04
B	0.0187	0.0354	0.73 ± 0.04
C	0.0187	0.0354	0.73 ± 0.04
D	0.0184	0.0353	0.72 ± 0.04

4. Discussion

The experimental results described in Sections 3.1 and 3.3 indicate that the step- and directly-quenched Cu–17.4Zn–13.0Al (at %) martensite is $M18R_1$ type and that all aging experiments in the present work were conducted in the $18R_1$ martensite state. The directly-quenched $M18R_1$ martensite changes its structure parameters towards $N18R_1$ during short time (< 2 h) aging. This process is an irreversible, thermally activated process with a rather small activation energy $Q = 58\,\mathrm{kJ\,mol^{-1}}$ (0.60 eV). Scarsbrook, Cook and Stobbs [10] obtained an activation energy $Q = 87.3 \pm 2.5\,\mathrm{kJ\,mol^{-1}}$ (0.90 eV) measured from the fraction of martensite which has not been stabilized after directly-quenching and aging in the martensite state with different aging time and temperatures. Mantel, Rapacioli and Guénin [19] obtained the migration energy $Q = 0.88 \pm 0.05$ eV ($85\,\mathrm{kJ\,mol^{-1}}$) of the vacancies in the disordered martensite by measuring the 77 K electrical resistivity changes. On the other hand, Van Humbeeck, Segers and Delaey [21] determined the vacancy migration energy in the Cu–Zn–Al parent phase to be $E_m = 0.66 \pm 0.02$ eV by positron annihilation measurements. Kennon, Danne and Middleton [22] reported the activation energy of the parent phase aging in a Cu–Zn–Al alloy to be 0.76 eV obtained from the increase in hardness, the loss of shape memory and the change of the M_s, M_f, A_s and A_f temperatures during aging at temperatures between 473 and 723 K. Our activation energy 0.60 eV resembles that of the parent phase aging rather than that of the martensite aging.

According to Equation 7 and using the fitted values listed in Table IV, the relaxation time at 345 K, which is lower than A_s temperature, should be $\tau(345\,\mathrm{K}) = 49$ h. Nonetheless the line-pairs splitting of the step-quenched martensite remains invariant after 49 h aging at 345 K. This fact indicates that the aging kinetics of the step-quenched martensite is much lower than the directly-quenched martensite. This is

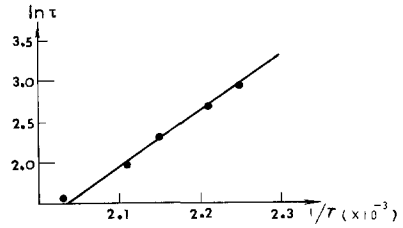

Figure 5 Plot of ln τ against $1/T$.

obviously because of the much lower vacancy concentration for the step-quenched specimen.

TEM observations on the domain size in the present work are in good agreement with reference [10] and may be explained as follows: the cooling rate during directly-quenching is much larger than step-quenching, hence the supercooling is larger for A2 → B2 → DO_3 transitions. Therefore, there are more nuclei of the order domains in the parent phase for the directly-quenching treatment, which results in the domains being smaller. These observations reveal that the A2 → B2 → DO_3 order transitions are indeed a nucleation and growth process. On the other hand, the directly-quenched martensite is always $M18R_1$ type. This indicates that the B2 → DO_3 order transition can not be completely suppressed by rapid cooling.

The present work is the first to measure the effect of the thermal treatment on the degree of DO_3-derived ordering and its variation during martensite aging. The higher DO_3-derived order degree for the step-quenched martensite in comparison with the directly-quenched one, as revealed by the X-ray quantitative measurement, may be explained by considering that the step-quenching temperaure of 433 K is lower than the B2 → DO_3 critical temperature $T_c(DO_3)$ = 540 K [23, 24]. The experiments described in Section 3.4. indicate that during short time aging in the martensite state, the change of the degree of DO_3-derived order lies in the limit of 5% coming from the statistical error. Hashiguchi *et al* [13] found a decrease in 6% of the B2-derived order degree in a Cu–Zn–Al martensite after 10^7 sec aging at RT. On the other hand, Tadaki, Tokoro and Shimizu [25] found a M9R type monoclinic martensite in a binary Cu–Zn alloy. The values of parameters of β = 88.43° and x = 1/2.79 = 0358 for this martensite correspond to the almost perfect B2-derived order. This means that the variation of the structure parameters of $18R_1$ martensite during aging after directly-quenching, as listed in Table II, is very large, which would correspond to a half of the difference between perfect B2-derived order and perfect disorder (or perfect DO_3-derived order) if there were some relationship between the structure parameters and the order degree. Thus we conclude that the substantial variation of the structure parameters of $18R_1$ martensite during aging is not due to the minor, if any, variation of the long range order degree of the martensite.

One possible explanation of the variation of the lattice parameters of the $18R_1$ martensite during aging in the martensite state is as follows: the thermodynamically most stable $18R_1$ martensite is nearly the $N18R_1$ type, i.e., $\beta \cong 90°$, $\varphi \cong 60°$, $x \cong \frac{1}{3}$. During the martensitic transformation, the (1 1 0) plane of the parent phase undergoes large distortion: φ angle decreases from 70.5° to nearly 60°. The strain energy introduced in such a way means that the structure of $18R_1$ martensite transformed directly from the parent can not be the most stable structure, but an intermediate structure with $\varphi > 60°$, $\beta < 90°$ and $x > \frac{1}{3}$. During martensite aging, thermal activation may help the martensite to change its structure towards the most stable one. Considering the measured value of 0.60 eV of the activation energy, it is reasonable to suppose that during the aging process the excess quenched-in vacancies migrate to the parent–martensite and other boundaries. The coalescence of the vacancies at martensite boundaries promotes the relaxation of the internal strain and hence the variation of the structure of the $18R_1$ martensite towards its equilibrium state. The vacancy migration in the retained parent phase is much faster than that in the martensite and hence plays a major role. During the same period, the body migration of the vacancies in the martensite is negligible and hence has little effct on the reordering or disordering of the martensite.

Based on the above discussion we propose that there are more mechanisms of martensite stabilization. Besides the martensite boundary pinning and the lowering of the martensite free energy by change of the order state, we would like to consider another mechanism proposed at first by Daleay *et al.* [3]: the variation of the lattice parameters leads to a change of the crystallographic relation between the martensite and the parent phase, especially the habit plane. Such a deviation of the aged martensite from its original invariant plane condition may prevent the martensite from being transformed reversibly until no reverse transition can occur before precipitation or decomposition of the martensite takes place.

5. Summary

1. The directly-quenched Cu–17.4Zn–13.0Al (at %) $M18R_1$ martensite changes its structure parameters towards those of $N18R_1$ martensite during short time aging. This is an irreversible, thermally activated process with a rather small activation energy Q = 58 kJ (0.60 eV) which resembles that of the parent phase aging. However, the structure parameters of the step-quenched $M18R_1$ martensite remain invariant owing to the much lower vacancy concentration.

2. The DO_3-derived long-range order degree of the step-quenched martensite is higher than that of the directly-quenched one. The substantial variation of the structure parameters of the directly quenched $M18R_1$ martensite during aging is not due to the minor, if any, variation of the long-range order degree of the martensite.

3. Both the B2- and the DO_3-derived domain sizes of the step-quenched martensite inherited from the parent phase are much larger than those of the directly-quenched and the directly-quenched and aged martensities. This is because direct quenching possesses a higher cooling rate, and hence a larger supercooling for A2 → B2 → DO_3 transitions.

4. From our studies we suppose that the thermodynamically most stable $18R_1$ martensite is nearly the $N18R_2$ type. The large strain energy introduced during such a martensitic transformation results in the situation that the structure of the $18R_1$ martensite transformed directly from the parent phase is an intermediate structure ($M18R_1$) with a lower strain energy. The rapid vacancy migration in the retained parent phase may help this martensite to vary its structure towards its equilibrium state. This variation leads to a change of the habit plane, and such a change may prevent the martensite from being transformed reverse in.

Appendix: Definition of the DO_3-derived long range order parameter S

For the sake of simplicity and noticing that the error would be very small when confusing the difference between Cu and Zn atoms in the case of X-ray and electron diffraction, we define the DO_3-derived long range order parameter S as follows: for the $18R_1$ martensite, there are four sublattices [20]. The sublattices 3 and 4 are occupied by Cu atoms irrespective of the DO_3-derived order degree S. In the perfect DO_3-derived order state ($S = 1$), all Al atoms lie at the sublattice 2, of which the remaining is occupied by Zn. When $S = 0$, the sublattices 1 and 2 have the same atomic occupation. Let c_{Cu}, c_{Zn} and c_{Al} be the atomic fractions of the Cu, Zn and Al atoms respectively with $c_{Cu} + c_{Zn} + c_{Al} = 1$, then the fractions of each atom on the sublattice 1 and 2 are as follows:

	Sublattice 1	Sublattice 2
Al	$(1 - S)2c_{Al}$	$(1 + S)2c_{Al}$
Zn	$(4c_{Al} + 2c_{Zn} - 1)S + 2c_{Zn}$	$-(4c_{Al} + 2c_{Zn} - 1)S + 2c_{Zn}$
Cu	$(1 + S)(2c_{Cu} - 1)$	$(1 - S)(2c_{Cu} - 1)$

Therefore, the partial structure factor expressing the contribution of the basal plane for the DO_3-derived order superreflections (when the index $k = 2n + 1$ with n being integer) [20] can be simplifed as

$$f_1 - f_2 = SF_b \qquad \text{(A1)}$$

with

$$F_b = 4(c_{Cu} - \tfrac{1}{2})f_{Cu} + 4(2c_{Al} + c_{Zn} - \tfrac{1}{2})f_{Zn} - 4c_{Al}f_{Al} \qquad \text{(A2)}$$

where $f_{Cu}, f_{Zn}, f_{Al}, f_1$ and f_2 are the atomic factors for Cu, Zn, Al, site 1 and site 2 respectively and F_b the partial structure factor for the perfectly ordered $18R_1$ martensite. From Equation A1 Equation 3 results.

Acknowledgement

Project supported by the National Natural Science Foundation of China.

References

1. M. AHLERS, in 'ICOMAT-86" (The Japan Institute of Metals, Sendai, 1986) p. 786.
2. G. SCARSBROOK, J. M. COOK and W. M. STOBBS, in "ICOMAT-82", edited by L. Delaey and M. Chandrasekaran (Leuven, 1982) p. 703.
3. L. DELAEY, T. SUSUKI and J. VAN HUMBEECK, *Scripta Metall.* **18** (1984) 899.
4. R. WANG, J. GUI, Y. ZHAO, X. ZHAO, H. ZHANG and G. ZHANG, in "ICOMAT-86" (The Japan Institute of Metals, Sendai, 1986) p. 822.
5. S. S. TAN, X. J. GAO and J. C. HUANG, *ibid.* p. 844.
6. X. Y. LU and M. S. CAO, *ibid.* p. 856.
7. M. DE GRAEF, J. VAN HUMBEECK and L. DELAEY, *ibid.* p. 850.
8. L. DELAEY, M. CHANDRASEKARAN, M. ANDRADE and J. VAN HUMBEECK, in Proceedings of the International Conference on Solid–Solid Phase Transformation, edited by H. I. Aaronson *et al.* (Pittsburgh, 1981) p. 1429.
9. G. SCARSBROOK and W. M. STOBBS, *Acta Metall.* **35** (1987) 47.
10. G. SCARSBROOK, J. M. COOK and W. M. STOBBS, *Metall. Trans. A.* **15A** (1984) 1977.
11. X. QI, B. JIANG and T. Y. HSU, in "Shape Memory Alloy '86", edited by Y. Chu, T. Y. Hsu and T. Ko (China Academic Publishers, Beijing, 1986) p. 297.
12. T. Y. HSU, *ibid.* p. 207.
13. Y. HASHIGUCHI, H. HIGUCHI, I. MATSUI, T. NIITANI, H. TOKUNOH and Y. IKAI, in ICOMAT-86 (The Japan Institute of Metals, Sendai, 1986) p. 832.
14. M. DE GRAEF, J. VAN HUMBEECK, M. ANDRADE and L. DELAEY, *Scripta Metall.* **19** (1985) 643.
15. M. DE. GRAEF, D. BRODDIN, J. VAN HUMBEECK and L. DELAEY, in Proceedings of the XIth International Congress on Electron Microscopy, Kyoto, 1986, p. 845.
16. J. M. COOK, M. A. O'KEEFE, D. J. SMITH and W. M. STOBBS, *J. Microsc.* **129** (1983) 295.
17. J. DUTKIEWICZ and J. MORGIEL, *J. Mater. Sci.* **21** (1986) 429.
18. K. SHIMIZU, in "Shape Memory Alloy '86", edited by Y. Chu, T. Y. Hsu and T. Ko (China Academic Publishers, Beijing, 1986) p. 15.
19. M. MANTEL, R. RAPACIOLI and G. GUÉNIN, in "ICOMAT-86" (The Japan Institute of Metals, Sendai, 1986) p. 880.
20. R. WANG, Y. ZHAO and J. GUI, *J. Electron Microscopy Technique* **7** (1987) 293.
21. J. VAN HUMBEECK, D. SEGERS and L. DELAEY, *Scripta Metall.* **19** (1985) 477.
22. N. F. KENNEN, D. P. DANNE and L. MIDDLETON, *Metall. Trans. A* **13A** (1982) 551.
23. T. SUZUKI, Y. FUJII, R. KOJIMA and A. NAGASAWA, in "ICOMAT-86" (The Japan Institute of Metals, Sendai, 1986) p. 874.
24. A. PLANES, G. GUÉNIN and J. L. MACQUERON, *J. Phys. F: Met. Phys.* **15** (1985) 1203.
25. T. TADAKI, M. TOKORO and K. SHIMIZU, *Trans. JIM* **16** (1975) 285.

Received 11 October 1988
and accepted 13 April 1989